View metadata, citation and similar papers at core.ac.uk

brought to you by CORE

provided by IntechOpen

We are IntechOpen, the world's leading publisher of Open Access books Built by scientists, for scientists

4,800
Open access books available

122,000
International authors and editors

135M
Downloads

154
Countries delivered to

Our authors are among the

TOP 1%
most cited scientists

12.2%
Contributors from top 500 universities

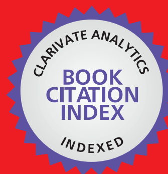

WEB OF SCIENCE™

Selection of our books indexed in the Book Citation Index in Web of Science™ Core Collection (BKCI)

Interested in publishing with us? Contact book.department@intechopen.com

Numbers displayed above are based on latest data collected.
For more information visit www.intechopen.com

14

Air Cooling Module Applications to Consumer-Electronic Products

Jung-Chang Wang[1] and Sih-Li Chen[2]
[1]*National Taiwan Ocean University*
[2]*National Taiwan University*
Taiwan, R.O.C.

1. Introduction

The purpose of this chapter is to describe how a air-cooling thermal module is comprised with single heat sink, two-phase flow heat transfer modules with high heat transfer efficiency, to effectively reduce the temperature of consumer-electronic products as Personal Computer (PC), Note Book (NB), Server including central processing unit (CPU) and graphic processing unit (GPU), and LED lighting lamp of smaller area and higher power. The research design concentrates on several air-cooling thermal modules. For air cooling, the extended surface, such as fin is usually added to increase the rate of heat removal. The heat capacity from heat source conducted and transferred through heat sink to the surroundings by air convection. Thus, the aim of adding fin is to help dissipate heat flow from heat source. The air convection heat transfer mechanism was shown in the figure 1, which can be separated into forced and free/nature convection through dynamic fluid device as fan. The chapter is divided into three parts; first part discusses optimum, performance analysis and verification of a practical convention parallel plate-fin heat sink. Second part employs two-phase flow heat transfer devices, such as heat pipe, thermosyphon and vapor chamber comprised with heat sink to consumer-electronic products. The last part utilizes air-cooling thermal module in other industrial areas including injection mold and large motor.

A conventional plate-fin heat sink is composed of a plate-fin heat sink and a fan. Thermal resistance network is often employed to analyze the thermal model and system in the industry. The overall thermal resistance includes interface resistance, base-conduction resistance, and convective resistance. It is worth developing a model for a conventional air-cooling device that takes heat sink configuration and airflow conditions into account in order to predict the device's thermal performance when developing laminar-, transition-, and turbulent-flow regimes. Although, solving the high heat capacity of electronic components has been to install a heat sink with a fan directly on the heat source, removing the heat through forced convection. Increasing the fin surface and fan speed are two direct heat removal heat sink in order to solve the ever increasing high heat flux generated by heat source from consumer-electronic products. They can reduce the total thermal resistance from 0.6 °C/W to 0.3 °C/W. Lin & Chen (2003) and Wu et al. (2011) has been developed an analytical all-in-one asymptotic model to predict the hydraulic and thermal performance of

a practical heat sink including a rectangular base plate and parallel fins with a non-uniform heat source, which proposed for a wide range of Reynolds and Nusselt numbers, including laminar, transition, and turbulent flows. However, increasing the surface area results in an increase in cost and boosting the fan speed results in noise, vibration and more power consumption, which increases the probability of failure to consumer-electronic components. Its total thermal resistance is usually over 0.3 °C/W not adjust high heat capacity; A two-phase flow heat transfer module with high heat transfer efficiency, to effectively reduce the temperature of heat sources of smaller area and higher power.

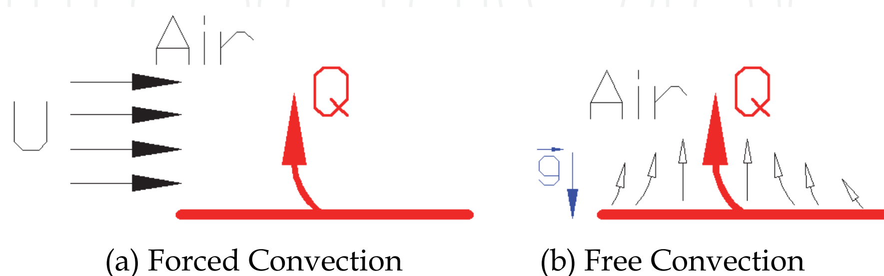

Fig. 1. Air convection mechanism

In recent years, technical development related with the application of two-phase flow heat transfer assembly to thermal modules has become mature and heat pipe-based two-phase flow heat transfer module is one of the best choices (Wang, 2008). A heat sink with embedded heat pipes transfers the total heat capacity from the heat source to the base plate with embedded heat pipes and fins sequentially, and then dissipates the heat flow into the surrounding air. Wang et al. (2007) have experimentally investigated the thermal resistance of a aluminium heat sink with horizontal embedded two and four U-shape heat pipes of 6 mm diameter; they showed that two heat pipes embedded in the base plate carry 36 percent of the total dissipated heat capacity from Central Process Unit (CPU), while 64% of heat was delivered from the base plate to the fins. Furthermore, when the CPU power was 140 W, the total thermal resistance was at its minimum of 0.27 °C/W. And using four embedded heat pipes carry 48 percent of the total dissipated heat capacity from CPU; the total thermal resistance is under 0.24 °C/W. The total thermal resistance of the heat sink with embedded heat pipes is only affected by changes in the base to heat pipes thermal resistance and heat pipes thermal resistance over the heat flow path; that is, the total thermal resistance varies according to the functionality of the heat pipes. If the temperature of the heat source is not allowed to exceed 70 °C, the total heating powers of heat sink with two and four embedded heat pipes will not exceed 131 Wand 164 W respectively. The superposition principal analytical method for the thermal performance of the heat sink with embedded heat pipes is completely established (Wang, 2009). The thermal performance of a heat sink with embedded heat pipes has been developed a Windows program for rapidly calculating through Visual Basic commercial software (Wang, 2010a). The computing core of this Windows program employs the theoretical thermal resistance analytical approach with iterative convergence to obtain a numerical solution. The estimation error between the numerical and experimental solutions is less than ±5%. The optimum inserting heights with total fin height are also obtained through the fitting curves generated in the program. From this Windows program, the optimum height of the embedded heat pipes inserted through fins is 21mm and 15mm for one pair and two pairs of embedded heat pipes, respectively. If

the heat sink is considered in different orientations with respect to gravity, the results may be different. Finally, this Windows program has the advantage of rapidly calculating the thermal performance of a heat sink with embedded heat pipes installed horizontally with a processor by inputting simple parameters.

Moreover, one set of risers of the L-shape heat pipes were functioning as the evaporating section while the other set acted as condensing section. Six L-type heat pipes are arranged vertically in such a way that the bottom acts as the evaporating section and the risers act as the condensing section (Wang, 2011b). It describes the design, modeling, and test of a heat sink with embedded L-shaped heat pipes and plate fins. This type of heat sink is particularly well suited for cooling electronic components such as microprocessors using forced convection. The mathematical model includes all major components from the thermal interface through the heat pipes and fins. It is augmented with measured values for the heat pipe thermal resistance. A Windows-based computer program also uses an iterative superposition method to predict the thermal performance. The sum of the bypass heating power ratios is 14.4% for Q1 and Q2, 20.8% for Q3 and Q4, and 52% for Q5 and Q6, obtained using both the experimental results and the software program based on VB6.0. Thermal performance testing shows that a representative heat sink with six heat pipes will carry 160W and has reached a minimum thermal resistance of 0.22 °C/W. The computer software predicted a thermal resistance of 0.21 °C/W, which was within 5% of the measured value. Moreover, the total thermal resistance of the heat sink with six embedded L-type heat pipes is only affected by changes in the base to heat pipes thermal resistance and heat pipes thermal resistance over the heat flow path. That is, the total thermal resistance varies according to the functionality of the L-type heat pipes. The index of the thermal performance of a heat pipe for a thermal module manufacturer is the temperature difference between the evaporation and condensation sections of a single heat pipe and maximum heat capacity. The maximum heat capacity reaches the highest point, as the amount of the non-condensation gas of a heat pipe is the lowest value and the temperature difference between evaporation and condensation sections is the smallest one. The temperature difference is under 1°C while the percentage of the non-condensation gas is less than 8×10^{-5}%, and the single heat pipe has the maximum heat capacity (Wang, 2011a). To establish a practical quick methodology that can effectively and efficiently determine the thermal performances of heat pipes so as to substitute the use of the conventional steady-state test. A novel dynamic test method is originated and developed (Tsai et al. 2010a). With a view toward shortening the necessary time to examine the thermal performances of heat pipes, a novel dynamic test method is originated and compared to the conventional steady-states test. The dynamic test can be adopted as a serviceable method to determine thermal performances of heat pipes. Only 10-15 min is necessary to examine a heat pipe using the dynamic test. This is much more efficient than the steady-state test and would be greatly beneficial to the notebook PC industry or other heat dissipation technologies that use heat pipes.

Liquid cooling technology employs the excellent thermal performance of liquid to quickly take away the heat capacity from a heat source. The method by which liquid contacts the heat source can be divided into two types, including immediacy and mediacy. And thermoelectric cooler (TEC) has been applied to electronic cooling with its advantages of sensitive temperature control, quietness, reliability, and small size. Thermoelectric cooler is regarded as a potential solution for improving the thermal performances of cooling devices on the package. Huang et al. (2010) have combined TEC and water-cooling device to

investigate the thermal performance. An analytical model of the thermal analogy network is provided to predict the cooling capability of the thermoelectric device. The prediction by the theoretical model agrees with the experimental results. Increasing the electric current not only enhances the Peltier effect, but also increases Joule heat generation of the TEC. Therefore, an optimum electric current of 7 A is determined to achieve the lowest overall thermal indicator at a specific heat load. A water-cooling device with a TEC is helpful to enhance the thermal performance when the heat load is below 57 W. Comparing with thermoelectric air-cooling module for electronic devices (Chang et al. 2009), the optimum input currents are from 6 A to 7 A at the heat loads from 20W to 100 W. The result also demonstrates that the thermoelectric air-cooling module performs better performance at a lower heat load. The lowest total temperature difference-heat load ratio is experimentally estimated as 0.54 °C/W at the low heat load of 20 W, while it is 0.664 °C/W at the high heat load of 100 W. In some conditions, the thermoelectric air-cooling module performs worse than the air cooling heat sink only.

In indirect liquid cooling technology, the outer surface of the chamber containing the working fluid makes contact for the required cooling of the electronic components. The heat capacity transfers to the working fluid through the chamber for heat dissipation. The driving force can be divided into active and passive by the way of the working fluid. The main objective of a passive liquid cooling system is not to use components, such as a pump, to drive the working fluid cycle. At present, the development of passive and indirect liquid cooling technology includes heat pipes, and vapor chambers composed of thermosyphon thermal modules, which have been applied in a variety of high heat-flux electronic components. Due to the demand for different heat transfer components, a two-phase thermosyphon can be divided into closed-loop and closed types. Two-phase closed-loop thermosyphon thermal modules are all two-phase change heat transfer components, their operating principle is to transfer heat capacity for cooling purposes by boiling and condensation of the phase change of the working fluid. Thus, finding how to enhance the boiling mechanism and reduce the thickness of condensation film will determine the operating thermal performance of the thermal module. This module offers the same vapor and liquid flow direction without the limitations of traditional heat pipes. Dissipation of the heat capacity of the heat source is conducted by forced convection to the atmosphere around the condenser section. This is because the vapor pressure in the evaporator section through the connecting pipe to condensation caused by the pressure drop. Therefore, the two-phase closed-loop thermosyphon thermal module has a water level difference within the evaporator and condenser. Furthermore, the different cooling fin groups in the thermal module and the condensing capacity of the evaporator section and condenser section are in contact with the working fluid of the different cross-sectional areas. Therefore, the water level is significantly different on the left and right sides of the evaporation section and the condensation section of the internal working fluid of the two-phase closed-loop thermosyphon thermal module. Therefore, it is important to note the vapor pressure difference caused by the water level in the design of this type of thermal module.

The two-phase closed thermosyphon cooling system is combined with a vapor-chamber formed evaporator to gain the advantages of vapor chamber (Chang et al. 2008; Tsai et al. 2010b). The facility allows different structured surfaces to be applied, and the effects of heating powers, fill ratios of working fluid, and types of evaporation-enhanced surfaces on the performance of the two-phase closed thermosyphon vapor-chamber system are

investigated and discussed. A thermal resistance net work is developed in order to study the effects of heating power, fill ratio of working fluid, and evaporator surface structure on the thermal performance of the system. Other words, the experimental parameters are different evaporation surfaces, fill ratios of working fluid and input heating powers. The results indicate that either a growing heating power or a decreasing fill ratio decreases the total thermal resistance, and the surface structure also influences the evaporator function prominently. An optimum overall performance exists at 140W heating power and 20% fill ratio with sintered surface, and the corresponding total thermal resistance is 0.495 °C/W. A growing fill ratio significantly enlarges the saturation pressure and temperature of the system, and results in worse performance of the condenser. The heat transfer mechanism of the three surfaces all can be ranked as boiling dominated. The result shows that the evaporation resistance and the condensation resistance both grow with increasing heating power and decreasing fill ratio. Flooding is found at the fill ratio of 20% with the evaporation surface noted Etched Surface 2 when heating power is above 120 W. Flooding phenomenon is caused by the opposite flow direction of vapor and liquid in a closed two-phase system. According to the result, the lowest total thermal resistance is 0.65 °C/W by the evaporation surface noted Etched Surface 2 at 30% fill ratio. Flooding phenomenon occurs as the system operated at low fill ratio and high input heating power. The flooding operation point for this system has been predicted by correlation, and the prediction is closed to the experimental results.
Vapour has advantages of fast, large amount and safety. Another two-phase heat transfer device is the Vapour Chamber (V.C.) inside vapour-liquid working, which has better thermal performance than metallic material in a large footprint heat sink. The overall operating principle of V.C. is defined as follows: at the very beginning, the interior of the vapor chamber is in the vacuum, after the wall face of the cavity absorbing the heat from its source, the working fluid in the interior will be rapidly transformed into vapour under the evaporating or boiling mechanism and fill up the whole interior of the cavity, and the resultant vapor will be condensed into liquid by the cooling action resulted from the convection between the fins and fan on the outer wall of the cavity, and reflow to the place of the heat source along the capillary structure. The effectiveness and better thermal performance of vapour chamber has been already confirmed according up-to-date researches and mass production application in server system and VGA thermal module. Moreover, vapour chamber-based thermal module has existed in the thermal-module industry for a year or so especially in server application (Wang & Chen 2009; Wang 2010; Wang et al. 2011a). A novel formula for effective thermal conductivity of vapor chamber has been developed by use of dimensional analysis in combination with thermal-performance experimental method (Wang & Wang 2011b). It respectively discussed these values of one, two and three-dimensional effective thermal conductivity and compared them with that of metallic heat spreader. For metallic materials as the heat spreaders, their thermal conductivities have constant values when the operating temperature varies not large. The thermal conductivities of pure cooper and aluminum as heat spreaders are 401 W/m°C and 237 W/m°C at operating temperature of 27 °C, respectively. When the operating temperature is 127 °C, they are 393 W/m°C and 240 W/m°C, respectively. Results show that the two and three-dimensional effective thermal conductivities of vapor chamber are above two times higher than that of the copper and aluminum heat spreaders, proving that it can effectively reduce the temperature of heat sources. The maximum heat flux of the vapor

chamber is over 800,000 W/m^2, and its effective thermal conductivity will increase with input power increasing. Thermal performance of V.C. is closely relate to its dimensions and heat-source flux, in the case of small area vapour chamber and small heat-source flux, the thermal performance will be less than that of pure copper material. It is deduced from the novel formula that the maximum effective thermal conductivity is above 800 W/m°C, and comparing it with the experimental value, the calculating error is no more than ±5%.

A vapour chamber is a two-phase heat transfer components with a function of spreading and transferring uniformly heat capacity so that it is ideal for use in non-uniform heating conditions especially in LEDs (Wang 2011c). The solid-state light emitting diode (SSLED) has attracted attention on outdoor and indoor lighting lamp in recent years. LEDs will be a great benefit to the saving-energy and environmental protection in the lighting lamps region. A few years ago, the marketing packaged products of single die conducts light efficiency of 80 Lm/W and reduces the light cost from 5 NTD/Lm to 0.5 NTD/Lm resulting in the good market competitiveness. These types of LED lamps require combining optical, electronic and mechanical technologies. Wang & Wang (2011a) introduce a thermal-performance experiment with the illumination-analysis method to discuss the green illumination techniques requesting on LEDs as solid-state luminescence source application in relative light lamps. The temperatures of LED dies are lower the lifetime of lighting lamps to be longer until many decades. The thermal performance of the LED vapour chamber-based plate is many times than that of LED copper- and aluminum- based plate (Wang & Huang 2010). The results are shown that the experimental thermal resistance values of LED copper- and vapour chamber-based plate respectively are 0.41 °C/W and 0.38 °C/W at 6 Watt. And the illumination of 6 Watt LED vapour chamber-based plate is larger 5 % than the 6 Watt. Thus, the LED vapour chamber-based plate has the best thermal performance above 5 Watt. The thermal performance of the LED vapor chamber-based plate is worse than that of the LED copper-based plate of less than 4 Watts. In additional to having the best thermal performance above 5 Watts, the luminance of the LED vapor chamber-based plate is the highest. The temperature of the LED rises about 12 °C per Watt (Wang 2011d). Wang et al. (2010b) utilizes experimental analysis with window program VCTM V1.0 to investigate the thermal performance of the vapor chamber and apply to 30 Watt high-power LEDs. Results show that the maximum effective thermal conductivity is 870 W/m°C, and comparing it with the experimental value, the calculating error is no more than ±5%. And the LED vapor chamber-based plate works out hot-spot problem of 30 Watt high-power LEDs, successfully. Thermal performance of the thermal module with the vapour chamber can be determined within several seconds by using the window program VCTM V1.0, exactly. The maximum heat flux of the vapor chamber is over 100 W/cm^2, and the thermal performance of the LED vapor chamber-based plate is better than that of the LED aluminum based-plate above 10 °C and has the highest effective thermal conductivity of 965 W/m°C at 187.5 W/cm^2.

In last, air-cooling thermal module in large-scale industrial enclosed air-to-air cooled motor with a capacity of 2350 kW is experimentally and numerically investigated (Chen et al. 2009; Chang et al. 2010). The models of the fan and motor have been implemented in a Fluent/Flow-3D software packages to predict the flow and temperature fields inside the motor. The modified design can decrease the temperature rise by 6 °C in both the stator and rotor. Wang et al. (2011b) uses the local heating mechanism, along with the excellent thermal performance of vapour chamber, to analyze and enhance the strength of products formed

after insert molding process. These results indicate that, the product formed by the local heating mechanism of vapour chamber can reduce the weld line efficiency and achieve high strength, which passed the standard of 15.82 N-m torque tests, with a yield rate up to 100%. In this study, a vapor chamber-based rapid heating and cooling system for injection molding to reduce the welding lines of the transparent plastic products is proposed. Tensile test parts and multi-holed plates were test-molded with this heating and cooling system. The results indicate that the new heating and cooling system can reduce the depth of the V-notch as much as 24 times (Tsai et al. 2011; Wang & Tsai 2011). The key results show that the proper air-cooling modules are important. There are several theoretical models of air-cooling modules developed to predict their thermal performance respectively. Finally, these results show that the prediction by the model agrees with the experimental data. The theoretical models with empirical formula have coded by Virtual Basic version 6.0 to develop window programs and convenience for industrials in this chapter.

2. Optimum and performance analysis of a parallel plate-fin heat sink

A conventional air-cooling device combining a plate-fin heat sink and forced convection with cost-competitive advantages and simple and reliable manufacturing processes, has been widely used in electronic cooling for the past several years. This practical heat sink is composed of a plate-fin heat sink and a fan, which attached to the heat source with proper thermal interface material and is cooled by airflow caused by the fan. The heat is conducted through the thermal interface, spreads into the base plate and the fins of the heat sink, and then transfers into the environment by airflow. A thermal resistance network includes interface resistance, base-conduction resistance, and convective resistance. It is worth developing a model for a conventional air-cooling device that takes heat sink configuration and airflow conditions into account in order to predict the device's thermal performance when developing laminar-, transition-, and turbulent-flow regimes. A plate-fin heat sink has been developed to predict the hydraulic and thermal performance in the following paragraphs. This all-in-one asymptotic model was proposed for a wide range of Reynolds and Nusselt numbers, including laminar, transition, and turbulent flows. It can predict pressure drops with accuracy within 6% and clarify the heat transfer coefficients within 15% of error range. Furthermore, optimization in geometry with the present model is achieved. The optimal values contain fin height, spacing and thickness, and base thickness, width and length. Using constrictive ratio and apparent interface ratio to interpret equivalent heat source area and maximal heat flux on source-to-sink contacting surface, the non-uniform heat source problem can be simplified as an equivalent uniform heat source problem. Then by using the existed correlations the present model can calculate the overall thermal resistance as a function of heat sink geometry, properties, interface conditions, and airflow velocity. An experimental investigation is performed to verify the theoretical model. Prediction results show good agreement with experimental measurements over a number of testing units.

2.1 Practical pressure drops model for a conventional plate-fin heat sink

The analysis for the extended fins array is conducted first to derive a working fluid-pressure drop across the heat sink and the effective convection coefficient. Analysis of the friction factor and heat-transfer coefficient in the channel flow evaluates whether the coolant flow is

laminar or turbulent. The critical Reynolds number, Re_c, is used to determine the flow regime. It has been found that the laminar to turbulent transition is not a sudden phenomenon, but occurs over a range of Reynolds numbers, $Re_c < Re < 4000$, for rectangular-duct flow. For numerical calculation purposes, a curve-fitting correlation by abrupt-entrance data is presented below as Eq. (1). The fitting error is within 8% to 1.6%, in a range of $0< \alpha < 1$:

$$Re_c = 1.6(\ln\alpha)^3 + 6.6(\ln\alpha)^2 - 161.6(\ln\alpha) + 2195 \quad (1)$$

Where α is the aspect ratio, and b and a are the fin spacing and the fin height, respectively.
The pressure drop in the plate heat sink can be divided into two parts: the friction term, and the term due to the change of flow section. The heat sink pressure drop is considered as Eq. (2), where f_{app} is the fanning-friction factor, K_c and K_e are contraction and expansion pressure loss coefficients, u_m is the coolant velocity in the channel, and L and D_h are the channel length and hydraulic diameter, respectively.

$$\Delta P = \left(4 f_{app}\frac{L}{D_h} + K_c + K_e\right)\cdot\frac{1}{2}\rho u_m^2 \quad (2)$$

In order to obtain a general friction factor correlation for the rectangular-duct flow over developing laminar-, transition-, and turbulent-flow regimes, an asymptotic solution is given as

$$f_{app} = \left(f_{lam}^n + f_{turb}^n\right)^{1/n} = \left\{\left[\frac{24}{Re}\left(1 - 1.4\alpha + 1.9\alpha^2 - 1.7\alpha^3 + \alpha^4 - 0.3\alpha^5\right)\right]^3 + \left[0.1\,Re^{-0.2}\left(\frac{x}{D_h}\right)^{-0.175}\right]^3\right\}^{1/3} \quad (3)$$

Where Re is the Reynolds number according to the hydraulic diameter. This correlation is predictive to within 14% to 6% accuracy.
Pressure loss due to an abrupt cross section change in the heat sink has been studied. Correlations of K_e and K_c for laminar-parallel plate ductsare used in this paper to evaluate pressure loss:

$$K_c = 0.8 - 0.4\left(\frac{b}{p}\right)^2 \quad (4)$$

$$K_e = \left(1 - \left(\frac{b}{p}\right)^2\right) - 0.4\left(\frac{b}{p}\right) \quad (5)$$

Where p is the fin pitch.

2.2 Heat transfer model for a conventional plate-fin heat sink

Using the same idea, an asymptotic approach is also conducted to obtain a general Nusselt number correlation for the laminar, transition, and turbulent flows. The asymptotic solution is given as

$$Nu = \left(Nu_{lam,dev}^{n} + Nu_{turb,dev}^{n} \right)^{1/n} \tag{6}$$

In order to obtain $Nu_{lam,dev}$ with three heating walls in a channel in Eq.(6), the present work first determined $Nu'_{lam,dev}$ with four heating walls. A general model evaluating Nu in the laminar-thermally developing regime of a noncircular duct with four heating walls is employed. The solution is given as the above equation predicts the heat-transfer capacity when four walls are being heated. However, in the present case, only three walls are heated, and the top wall is insulated. The Nusselt number for low Reynolds numbers with three walls heated is valid for $0 < \alpha < 1$ and predicts accuracy within 5%. $Nu_{turb,dev}$ employs the correlation provided and substitutes an equivalent diameter for the hydraulic diameter: In contrast to the laminar flow, no compensation for heat-transfer coefficient for three wall heating is required, since the turbulent mixing among the channel sections does quite well and significantly reduces the influence of the asymmetric boundary condition. After the prediction of Nu is obtained, h_m can also be determined. The bulk convection heat-transfer coefficient, h_m, is based on the log-mean temperature difference. According to the same power dissipation, the definitions of these two are exhibited below: convective heat-transfer coefficient (h_i) refers to the inlet temperature for predicting convection thermal resistance. The coefficient is based on the temperature difference between the heat sink and the inlet-fluid temperatures. Moreover, energy balance between the heat-transfer rate from the heat sink wall to the fluid and the increment rate of fluid enthalpy is considered, and then obtains the result in a relationship between h_m and h_i: The above-mentioned correlations of the Nusselt number and the friction factor employ fluid properties corresponding to the mean bulk temperature.

The above model combines two correlations of laminar and turbulent flows, and provides the friction factor and the Nusselt number for developing laminar, transition, and turbulent flows. Using the friction factor and the loss coefficient formula of parallel plates, this model can predict a pressure drop in a heat sink within errors from 13.71% to 8.47% against experimental data with an aspect ratio from 0.05 to 0.2. The Nusselt number has been proposed for convective heat-transfer prediction. This asymptotic solution predicts a Nusselt number within acceptable errors for transition and turbulent flows, namely 15% to 12%, but it predicts a higher Nusselt number of 7%. This study considers the convection heat transfer of fins, pressure drop, fin efficiency, effective heat-transfer coefficient, and conduction problems of the heat sink base, then derives a practical model predicting the thermal performance of the plate-fin heat sink, and develops a numerical program for calculating. Within acceptable accuracy, this model is useful to obtain a set of parameters for designing a plate-fin heat sink with expected performance.

3. Two-phase flow heat transfer devices

Liquid cooling technology employs the excellent thermal performance of liquid to quickly take away the heat capacity from a heat source. The method by which liquid contacts the heat source can be divided into two types, including immediacy and mediacy. Direct liquid cooling technology was first applied in the large area of a super computer in the 1960s. Which this type of technology, it is necessary to pay attention to the thermal shock effect. In indirect liquid cooling technology, the outer surface of the chamber containing the working fluid makes contact for the required cooling of the electronic components. The heat capacity

transfers to the working fluid through the chamber for heat dissipation. The driving force can be divided into active and passive by the way of the working fluid. The active type is like a pump in the liquid cooling system that drives the circulation loop of the working fluid, as used in laptop computer cooling systems. The disadvantages for the use of a pump are cost, lifespan, vibration, noise and other issues. Moreover, additional water-cooled assembly between the components increases the cost of thermal modules and reduces the reliability of electronic components. The main objective of a passive liquid cooling system is not to use components, such as a pump, to drive the working fluid cycle.
At present, the development of passive and indirect liquid cooling technology includes heat pipes, and vapor chambers composed of thermosyphon thermal modules, which have been applied in a variety of high heat-flux electronic components. These thermal modules also name two-phase flow heat transfer devices. This type of technology offers the following five benefits: 1. The module can transfer a lot of heat capacity with very small temperature gradient by the latent heat between the two-phase changes of liquid and gas. It has excellent thermal performance. 2. The flow in the system is driven by buoyancy and gravity/capillary force. These two driving forces are self-induced, so a flow-driven pump component is not necessary in this system. The thermal module itself has high reliability. 3. The two main components, including the evaporator and condenser, are separated and connected with pipes. Therefore, the arrangement of each component is much more flexible. Furthermore, fans can take advantage of existing systems. 4. The thermal module is composed of three parts, including the evaporator, connected piping and condenser. In addition, each of the three sections can be individually manufactured, providing high potential for extension. 5. It is highly feasible to combine more evaporators and condensers in a series of connections or parallel connections in the cooling system should extension be necessary. Therefore, this technology provides low cost manufacturing and installation of the modular.

3.1 Heat pipe

The heat pipe may mainly be differentiated for the evaporation section, the adiabatic section, and the condensation section and be regarded as the passive component of a self-sufficient vacuum closed system. The system which includes the capillarity structure and the filling of working fluid usually needs to soak through the entire capillarity structure. This research adopted a conventional steady-state test similar to previous works to investigate the steady-state thermal performances of heat pipes, and a detailed description of the experimental procedures and set-ups is introduced as follows. When the heat pipe works, the evaporation section of the heat absorption occurs in the capillarity structure. The working fluid gratifies as the vapor. The high temperature and pressure vapour is produced at the condensation section after the adiabatic section. The vapor releases heat and then condenses as the liquid. The working fluid in the condensation section is brought back to the evaporation section because of the capillary force in the capillarity structure. The capillary force has a relation with the capillarity structure, the viscosity, the surface tension, and the wetting ability. However, the capillary force and the high vapour pressure are the main driving force to make the circulation in the heat pipe. The working fluid in the heat pipe exists in the two-phase model of the vapor and liquid. The interface of the vapor and liquid's coexistence is regarded as the saturated state. It is usually assumed that the temperatures of the vapor and liquid are equal.

The heat pipe uses the working fluid with much latent heat and transfers the massive heat from the heat source under minimum temperature difference. Because the heat pipe has certain characteristics, it has more potential than the heat conduction device of a single-solid-phase. Firstly, due to the latent heat of the working fluid, it has a higher heat capacity and uniform temperature inside. Secondly, the evaporation section and the condensation section belong to the independent individual component. Thirdly, the thermal response time of the two-phase-flow current system is faster than the heat transfer of the solid. Fourthly, it does not have any moving components, so it is a quiet, reliable and long-lasting operating device. Finally, it has characteristics of smaller volume, lighter weight, and higher usability. Although the heat pipe has good thermal performance for lowering the temperature of the heat source, its operating limitation is the key design issue called the critical heat flux or the greatest heat capacity quantity. Generally speaking, we should use the heat pipe under this limit of the heat capacity curve.

There are four operating limits which are described as following. Firstly, the capillary limit, which is also called the water power limit, is used in the heat pipe of the low temperature operation. Specific wick structure which provides for working fluid in circulation is limiting. It can provide the greatest capillary pressure. Secondly, the sonic limit is that the speed of the vapour flow increases when the heat source quantity of heat becomes larger. At the same time, the flow achieves the maximum steam speed at the interface of the evaporation and adiabatic sections. This phenomenon is similar to the flux of the constant mass flow rate at conditions of shrinking and expanding in the nozzle neck. Therefore, the speed of flow in this area is unable to arrive above the speed of sound. This area is known for flow choking phenomena to occur. If the heat pipe operates at the limited speed of sound, it will cause the remarkable axial temperature to drop, decreasing the thermal performance of the heat pipe. Thirdly, the boiling limit often exists for the traditional metal, wick structured heat pipe. If the flow rate increases in the evaporation section, the working fluid between the wick and the wall contact surface will achieve the saturated temperature of the vapor to produce boiling bubbles. This kind of wick structure will hinder the vapour bubbles to leave and have the vapor layer of the film encapsulated. It causes large, thermal resistance resulting in the high temperatures of the heat pipe. Fourthly, the entrainment limit is that when the heat is increased and the vapor's speed of flow is higher than the threshold value, forcing it to bear the shearing stress in the liquid; vapor interface being larger than the surface tension of the liquid in the wick structure. This phenomenon will lead to the entrainment of the liquid, affecting the flow back to the evaporation section. Besides the above four limits, the choice of heat pipe is also an important consideration. Usually the work environment can have high temperature or low temperature conditions which will require a high temperature heat pipe or a low temperature heat pipe, accordingly. After deciding the operating environment, the material, internal sintered body, and type of working fluid for the heat pipe are determined. In order to prevent the heat pipe`s expiration, the consideration of the selection is very important.

3.2 Thermosyphon

This paragraph experimentally investigates a two-phase closed-loop thermosyphon vapor-chamber system for electronic cooling. A thermal resistance net work is developed in order to study the effects of heating power, fill ratio of working fluid, and evaporator surface structure on the thermal performance of the system. This study explored the relationship

between the vapor pressure and water level inside a two-phase closed-loop thermosyphon thermal module to acquire a theoretical model of the water level height difference of the thermal module through the analysis of basic condensing and boiling theory. Figure 2 shows the internal vapor pressure and water level through the heat source with the heating power Q, based on the entire experimental system. The internal vapour pressure and water level through the heat source with the heating power Q based on the entire experimental system. The entire physical system can be divided into four control volumes to resolve the vapour pressure and the friction loss of steam from the first control volume (C.V.1) to the third control volume (C.V.3), as revealed by formula (7). Furthermore, the liquid static pressure balance of the fourth control volume (C.V.4) is exhibited by formula (8). The range of C.V.1 is from the vapor chamber, including the area from the connecting pipe to the entrance of the condenser region, which encompasses the loss of steam pressure through the connecting pipe of the insulation materials. The range of C.V.2 is from the entrance to the outlet of the condenser, which involves a loss of steam pressure after the condenser. The scope of C.V.3 is from the outlet of the condenser to the connection surface of the vapor chamber, which entails a loss of steam pressure through the connecting pipe. The scope of C.V.4 is from the connection surface of the vapor chamber to the same high level in the connecting pipe of the vapor chamber.

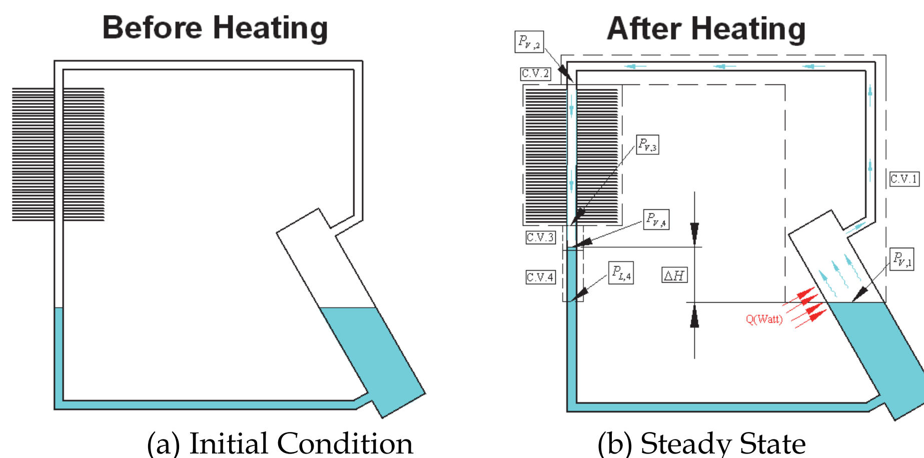

(a) Initial Condition (b) Steady State

Fig. 2. Relationship between vapour pressure and water level

$$P_{V,i} = P_{V,i+1} + \Delta P_{f,i} \tag{7}$$

Where $P_{V,i}$ is the vapor pressure of the ith control volume in this system, $P_{V,i+1}$ is the vapor pressure for the steam into (i+1)th control volume through ith control volume of the connecting pipe and $\Delta P_{f,i}$ is the friction loss of the pressure of steam flow.

$$P_{l,4} = P_{V,4} + \gamma_w \Delta H \tag{8}$$

where $P_{l,4}$ is the hydrostatic pressure of the C.V.4 of liquid, γ_w is the specific weight of liquid, ΔH is the height difference of the water level between the internal water level of the vapor chamber and the connecting pipe connected to the condenser.
The equations represented by C.V.1 to C.V.3 are all added up, and $P_{l,4}$ is equal to $P_{V,4}$ and substituting it into equation (8), ΔH can be obtained as shown in equation (9).

$$\Delta H = \left(1/\gamma_w \right) \cdot \sum_{i=1}^{3} \Delta P_{f,i} \tag{9}$$

From the equation (9), if there is no pressure drop loss for $\Delta P_{f,1}$ and $\Delta P_{f,3}$ of the pipeline and $\Delta P_{f,2}$ of the condenser, then the water level inside the vapour chamber and that connected to the condensation inside condenser will be the same. That is, ΔH is equal to zero.

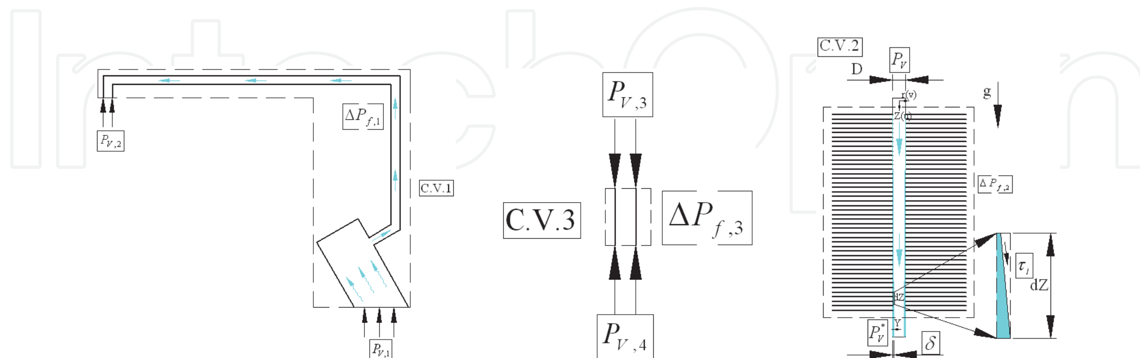

Fig. 3. Schematic diagram of the calculation of pressure drop loss (a) Pressure drop loss of the connecting pipe of C.V.1 (b) Pressure drop loss of the connecting pipe of C.V.3 (c) Pressure drop loss of the condenser

Figure 3(a) and 3(b) show the estimated method for $\Delta P_{f,1}$ and $\Delta P_{f,3}$ of the connecting pipe. According to a previous study, this can be calculated by formula (10).

$$\Delta P_{f,i} = f_i \cdot \frac{L_i}{D_i} \cdot \frac{1}{2} \cdot \rho_{v,i} \cdot V_{v,i}^2 \tag{10}$$

Where f_i is the friction coefficient generated by the steam flow through the pipes, L_i represents the equivalent length of the connecting pipe, D_i is the diameter of the connecting pipe and $\rho_{v,i}$ and $V_{v,i}$ represent the vapour density and speed respectively.
According to figure 3(c) and previous studies, the method for calculating $\Delta P_{f,2}$ considers the shear stress or the friction force at the gas-liquid interface with small control volume. Formula (11) can be attained based on momentum conservation.

$$(\delta - y) \cdot dZ \left(\rho_w g - \frac{dP}{dz} \right) + \tau_i \cdot dZ = \mu_w \left(\frac{dV}{dy} \right) \cdot dZ \tag{11}$$

Where δ is the film thickness of the liquid inside the condenser tube, ρ_w is the liquid density, μ_w is the dynamic viscosity of the liquid, τ_i is the shear stress at the gas-liquid interface, (dP/dz) is the pressure drop loss generated by the steam flow through the gas-liquid interface at the condenser, which can be expressed as equation (12).

$$-\left(\frac{dP}{dz} \right) = -\left(\rho_v g \right) + \left(\frac{4\tau_i}{D - 2\delta} \right) + \left(\frac{d\left(\dot{m}_v V_v + \dot{m}_w V_w \right)}{dz} \right) \tag{12}$$

In which, $\dot{m}_v$ and $\dot{m}_w$ represent the mass flow rate of the steam and liquid, respectively. V_v and V_w denote the speed of vapour and liquid. τ_i is the shear stress of the gas-liquid interface, as shown in equation (13) below.

$$\tau_i = 0.005\left(1+\frac{300\cdot\delta}{D}\right)\cdot\left(\frac{G^2\cdot x^2}{2\cdot\rho_v\cdot(1-4\frac{\delta}{D})}\right) \quad (13)$$

$\left(\frac{d\left(\dot{m}_v V_v + \dot{m}_w V_w\right)}{dz}\right)$ is the pressure drop produced by the mass flow rate of the gas-liquid interface, which can be expressed as in equation (14).

$$\frac{d\left(\dot{m}_v V_v + \dot{m}_w V_w\right)}{dz} = G^2\cdot\frac{d}{dz}\left[\left(\frac{x^2}{\rho_v\alpha}\right)+\left(\frac{(1-x)^2}{\rho_w(1-\alpha)}\right)\right] \quad (14)$$

Where G is the mass flow rate flux, x is the mass flow rate fraction and α is the ratio of the gas channel. Substituting equation (14) into equation (12), the integral of the range from zero to Z can be obtained by formula (15) as follows.

$$(P_V^* - P_V) = \left(\rho_v g Z\right) - \int_0^Z\left(\frac{4\tau_i}{D-2\delta}\right)dz - G^2\left(\int_0^Z\frac{d}{dz}\left[\left(\frac{x^2}{\rho_v\alpha}\right)+\left(\frac{(1-x)^2}{\rho_w(1-\alpha)}\right)\right]\right)dz \quad (15)$$

Substituting $\alpha = \frac{A_v}{A} = \left(\frac{D-2\delta}{D}\right)$ into the above equation, we can obtain the formula (16) after integration as follows.

$$\Delta P_{f,2} = (P_v - P_v^*) = G^2 D\left[\left(\frac{x^2}{\rho_v(D-2\delta)}\right)+\left(\frac{(1-x)^2}{2\rho_w\delta}\right)\right]+\int_0^Z\left(\frac{4\tau_i}{D-2\delta}\right)dz - \left(\rho_v g Z\right) \quad (16)$$

To calculate the right side of the integral term $\int_0^Z\left(\frac{4\tau_i}{D-2\delta}\right)dz$ of the above formula (16), first, assume that the internal film growth equation of the liquid is linear. Therefore, the assumed slope of SP can attain formula (17) as follows.

$$\delta = SP*Z \quad (17)$$

And let

$$\xi = \frac{\delta}{D} \quad (18)$$

Substituting equations (17) and (18) into equation (14), we can obtain formula (19) as follows.

$$\tau_i = 0.0001\cdot\left(\frac{G^2\cdot x^2}{2\cdot\rho_v}\right)\cdot\left(\frac{1+300\xi}{1-4\xi}\right) \quad (19)$$

Substituting equation (19) into the right side of the integral term $\int_0^Z \left(\frac{4\tau_i}{D-2\delta}\right)dz$ of equation (16), we can obtain formula (20) as follows.

$$\int_0^Z \left(\frac{4\tau_i}{D-2\delta}\right)dz = \left(\frac{0.005 \cdot G^2 \cdot x^2}{Sp \cdot \rho_v}\right)\left[151 \cdot \ln(1-\frac{2 \cdot Sp \cdot Z}{D}) - 76 \cdot \ln(1-\frac{4 \cdot Sp \cdot Z}{D})\right] \quad (20)$$

Finally, by substituting equation (20) back into formula (16), we can obtain $\Delta P_{f,2}$ with formula (21) as shown below.

$$\Delta P_{f,cv2} = G^2 D\left[\left(\frac{x^2}{\rho_v (D-2\delta)}\right) + \left(\frac{(1-x)^2}{2\rho_w \delta}\right)\right] - (\rho_v g Z) + \left(\frac{0.005 \cdot G^2 \cdot x^2}{Sp \cdot \rho_v}\right)\left[151 \cdot \ln(1-\frac{2 \cdot Sp \cdot Z}{D}) - 76 \cdot \ln(1-\frac{4 \cdot Sp \cdot Z}{D})\right] \quad (21)$$

The film thickness δ can be calculated by the formula (22) as follows.

$$\frac{4 \cdot Z \cdot \mu_w \cdot q''}{\rho_w \cdot (\rho_w - \rho_v) \cdot g \cdot h'_{fg}} = \delta^3 + \frac{4 \cdot \tau_i \cdot \delta^2}{3 \cdot (\rho_w - \rho_v) \cdot g} \quad (22)$$

In which

$$h'_{fg} = h_{fg} \cdot \left[1 + \left(\frac{3}{8}\right) \cdot \frac{C_{pw} \cdot \delta \cdot q''}{h_{fg} \cdot k_w}\right] \quad (23)$$

Where h_{fg} is the latent heat of the working fluid, C_{pw} is the constant pressure of the specific volume of the liquid; q'' is the input heat flux of the heat source and k_w is the thermal conductivity of the liquid.

We use Microsoft® Visual Basic™ 6.0 to write the computing interface resulting from the above empirical formula and calculated the thermal performance and the water level deficit inside the thermal module of the two-phase closed-loop thermosyphon. The programming flow chart is shown in Figure 4(a) and the final operation interface is shown in Figure 4(b). This study discusses the thermal performance of the two-phase closed-loop thermosyphon thermal module, and indirectly confirms that the working fluid reflows into the condenser by measuring the wall temperatures of the condenser, which results in the water level difference phenomenon within the system. Figure 5 shows the theoretical curve of the water level height difference for the entire closed thermal module system. The solid black line in the figure is the theoretical water level height difference based on the heat transfer theory of pool nucleate boiling and film condensation in this study. Comparing the two curves, we can accurately predict the same level with the height difference between the experimental curve before the heating power is less than 60W; however, beyond 60W, the water level height difference obtained in the experimental curve has tended to be horizontal, while the theoretical curve will increases with the heating power, the water level height difference increases only slightly.

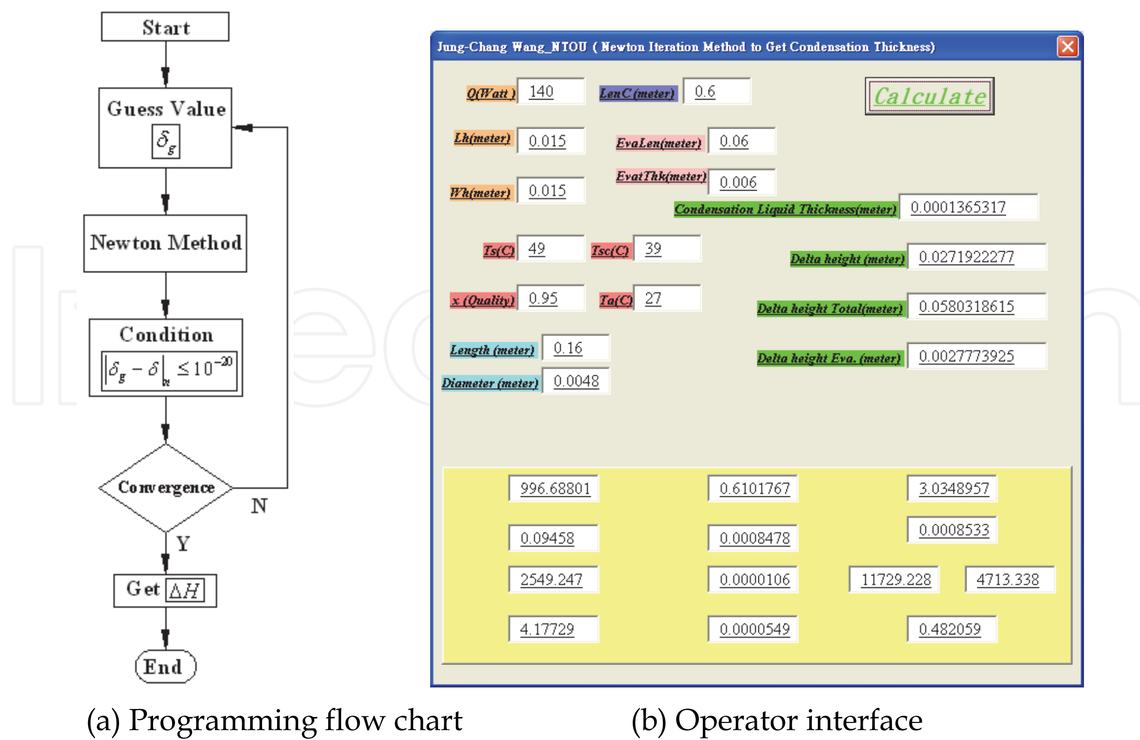

(a) Programming flow chart (b) Operator interface

Fig. 4. Programming and the operator interface

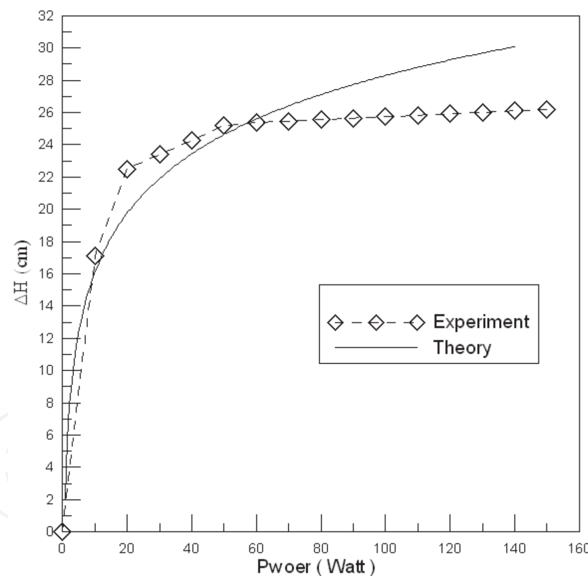

Fig. 5. The theoretical value of water level difference of vertical type

For the two-phase closed-loop thermosyphon cooling system, the micro-scale water level difference phenomenon resulting from the condensing and boiling vapor pressure difference between the evaporator and condenser sections based on the theories of pool nucleate boiling and film condensation and the validation of experimental method to measure the wall temperature of condenser. The height of the condenser of the two-phase closed-loop thermosyphon system can be shortened by 3.14cm by using the theoretical water level difference model. The working fluid within the two-phase closed-loop

thermosyphon system has different heights resulting from the vapor pressure difference between the evaporator and the condenser sections. This should be noted in the design of such two-phase heat transfer components. Finally, this study has established a theoretical height difference model for two-phase closed-loop cooling modules. This can serve as a reference for future researchers.

3.3 Vapor chamber

This study derives a novel formula for effective thermal conductivity of a vapor chamber using dimensional analysis in combination with a thermal-performance experimental method. The experiment selected water as the working fluid filling up in the interior of vapour chamber. The advantages of water are embodied in its thermal-physics properties such as extremely high latent heat and thermal conductivity and low viscosity, as well as its non-toxicity and incombustibility. The overall operating principle of the experiment is defined as follows: at the very beginning, the interior of the vapour chamber is in vacuum, after the wall face of the cavity absorbs the heat from its source, the working fluid in the interior will be rapidly transformed into vapour under the evaporating or boiling mechanism and fill up the whole interior of the cavity. The resultant vapour will be condensed into liquid by the cooling action resulted from the convection between the fins and fan on the outer wall of the cavity, and condensate will reflow to the wall at the heat source along the capillary structure as shown in figure 6.

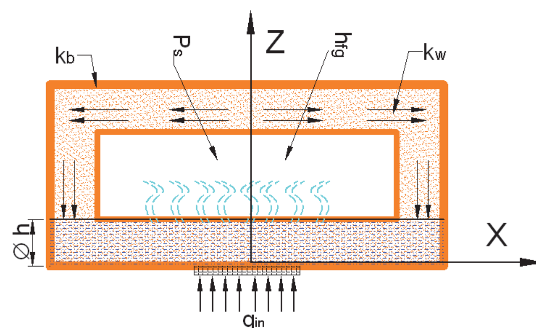

Fig. 6. Drawing of the vapor chamber

It discusses these values of one, two and three-dimensional effective thermal conductivity and compares them with that of metallic heat spreaders. Equation (24) indicates the effective thermal conductivity k_{index} of the vapor chamber, which is the result of the input heat flux q''_{in} multiplied thickness (t) of the vapour chamber divided by the temperature difference ΔT_{index}. The one-dimensional thermal conductivity (k_z) is when the index is equal to z and the temperature difference ΔT_z equals the central temperature (T_{dc}) on the lower surface minus that (T_{uc}) on the upper surface. The two-dimensional thermal conductivity (k_{xyd}) is when the index is equal to xyd and the temperature difference ΔT_{xyd} equals the central temperature (T_{dc}) on the lower surface minus mean surface temperature (T_{da}). The two-dimensional thermal conductivity (k_{xyu}) is when the index is equal to xyu and the temperature difference ΔT_{xyu} equals the central temperature (T_{uc}) on the upper surface minus mean surface temperature (T_{ua}). The three-dimensional thermal conductivity (k_{xyz}) is when the index is equal to xyz and the temperature difference ΔT_{xyz} equals mean surface temperature (T_{da}) on the lower surface minus that (T_{ua}) on the upper surface.

$$\mathrm{k_{index}} = {q''_{in} \cdot t} \Big/ {\Delta T_{index}} \tag{24}$$

One of major purposes of this study is to deduce the thermal performance empirical formula of the vapour chamber, and find out several dimensionless groups for multiple correlated variables based on the systematic dimensional analysis of the [F.L.T.θ.] in Buckingham Π Theorem, as well as the relationship between dimensionless groups and the effective thermal conductivity. Figure 6 is the abbreviated drawing of related variables of the vapour chamber to be confirmed in this article, and the equation (25) is the functional expression deduced based on related variables in Figure 6. The symbol k_{eff} in the equation is the value of effective thermal conductivity of the vapour chamber, the k_b is the thermal conductivity of the material made of the vapour chamber, the symbol k_w is the value of effective thermal conductivity of the wick structure of the vapour chamber, the unit of these thermal conductivities are W/m°C. The symbol h_{fg} is latent heat of working fluid which has unit of J/K. The P_{sat} is saturated vapour pressure of working fluid with unit of N/m^2. The t is the thickness of vapour chamber. Their unit is m. The symbol A is the area of vapour chamber and its unit is m^2.

$$K_{eff} = Function\left\{k_b, k_w, q''_{in}, h_{fg}, P_{sat}, t, A, \phi h\right\} \tag{25}$$

It can be inferred from equation (25) that there are nine related variables (symbol m equalling to 9), and the following equation (26) can be inferred by making use of [F.L.T.θ.] system (symbol r equalling to 4) to do a dimensional analysis of various parameters in the above-mentioned equation and combining the analysis result with the equation (25).

$$\left(\frac{k_{eff}}{k_b}\right) = \alpha \cdot \left(\frac{k_w}{k_b}\right)^{\beta} \cdot \left(\frac{q''_{in}}{P_{sat} \cdot h_{fg}{}^{0.5}}\right)^{\gamma} \cdot \left(\frac{A}{t^2}\right)^{\lambda} \cdot \left(\frac{\phi h}{t}\right)^{\tau} \tag{26}$$

The α,β,γ,λ,τ in the equation (26) indicate the constants determined based on the experimental parameters. We can know from the said equation (26) that effective thermal conductivity of the vapour chamber is related to controlling parameters of the experiment, fill-up number of the working fluid influencing Φh, volume of the cavity influencing t, input power and area of the heat source influencing q_{in}, area of the vapour chamber influencing A. Thus, this study is designed to firstly use thermal-performance experiment to determine the thermal performance and related experimental controlling parameters of the vapour chamber-based thermal, and sort them into the database of these experimental data, then combine with equation (26) to obtain the constants of the symbols α,β,γ,λ,τ. Let the constant α be 1. And these constants β,γ,λ,τ are equivalent to 0.13, 0.28, 0.15, and -0.54 based on some specified conditions in this research, respectively. This window program VCTM V1.0 was coded with Microsoft Visual Basic™ 6.0 according to the empirical formula and calculated the thermal performance of a vapor chamber-based thermal module in this study. These parameters affect its thermal performance including the dimensions, thermal performance and position of the vapor chamber. Thus it is very important for the optimum parameters to be selected to receive the best thermal performance of the vapor chamber-based thermal module. The program contains two main windows. The first is the selection window

adjusted in the program as the main menu as shown in Fig. 7. In this window, the type of the air direction can be chosen separately. The second window has five main sub-windows. There are four sub-windows of the input parameters for the thermal module as shown in Fig. 7. The first sub-window is the simple parameters of the vapor chamber including dimensions and thermal performance. Fig. 7 shows the second sub-window involving detail dimensions of a heat sink. The third and fourth sub-windows are the simple parameters containing input power of heat source, soldering material, and materials of thermal grease and performance curve of fan. All the input parameters required for this study of the window program were given and the window program starts. Later, the program examines the situation by pressing calculated icon. The fifth sub-window is the window showing the simulation results. In this sub-window, when it is pressed at calculate icon for making analysis of the thermal performance of a vapor chamber-based thermal module, we can see a figure as it is shown in Fig. 7.

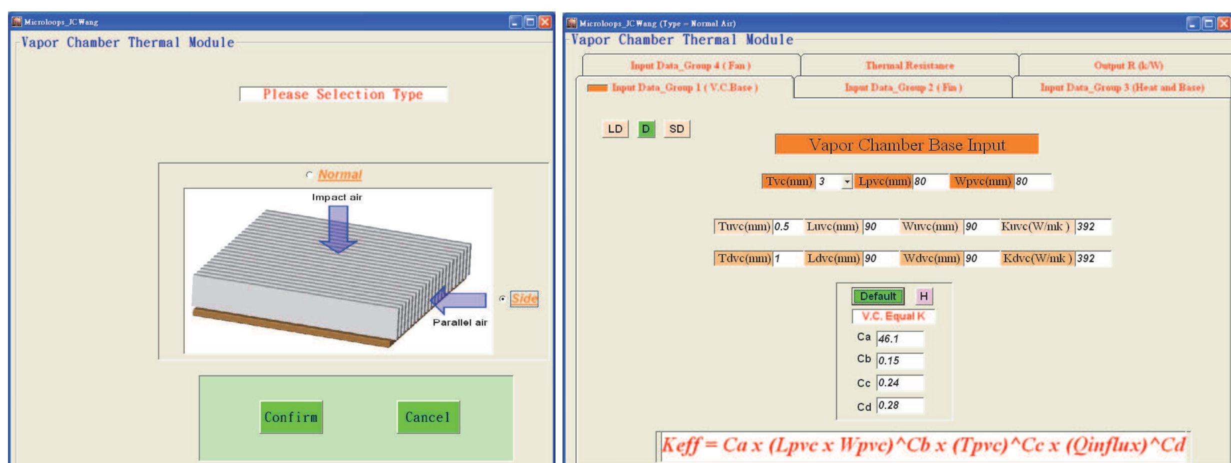

Fig. 7. Window program VCTM V1.0

Results show that the two and three-dimensional effective thermal conductivities of vapor chamber are more than two times higher than that of the copper and aluminum heat spreaders, proving that it can effectively reduce the temperature of heat sources. The maximum heat flux of the vapor chamber is over 800,000 W/m^2, and its effective thermal conductivity will increase with input power increases. It is deduced from the novel formula that the maximum effective thermal conductivity is above 800W/m°C. Certain error necessarily exist between the data measured during experiment, value deriving from experimental data and actual values due to artificial operation and limitation of accuracy of experimental apparatus. For this reason, it is necessary take account of experimental error to create confidence of experiments before analyzing experimental results. The concept of propagation of error is introduced to calculate experimental error and fundamental functional relations for propagation of error. During the experiment, various items of thermal resistances and thermal conductivities are utilized to analyze the heat transfer characteristics of various parts of thermal modules. The thermal resistance and thermal conductivity belong to derived variable and includes temperature and heating power, which are measured with experimental instruments. The error of experimental instruments is propagated to the result value during deduction and thus become the error of thermal resistance and thermal conductivity values. An experimental error is represented with a

relative error and the maximum relative errors of thermal conductivities defined are within ±5% of k_{index}. This study answered how to evaluate the thermal-performance of the vapor chamber-based thermal module, which has existed in the thermal-module industry for a year or so. Thermal-performance of the thermal module with the vapor chamber can be determined within several seconds by using the final formula deduced in this study. One- and two-dimensional thermal conductivities of the vapor chamber are about 100 W/m°C, less than that of most single solid-phase metals. Three-dimensional thermal conductivity of the vapor chamber is up to 910 W/m°C, many times than that of pure copper base plate. The effective thermal conductivities of the vapor chamber are closely relate to its dimensions and heat-source flux, in the case of small-area vapor chamber and small heat-source flux, the effective thermal conductivity are less than that of pure copper material.

4. Air-cooling thermal module in other industrial areas

Air-cooling thermal module in other industrial areas as large-scale motor and LEDs lighting lamp are discussed in the following paragraphs. And a vapour chamber for rapid-uniform heating and cooling cycle was used in an injection molding process system especially in inset mold products.

4.1 Injection mold

There are many reasons for welding lines in plastic injection molded parts. During the filling step of the injection molding process, the plastic melt drives the air out of the mold cavity through the vent. If the air is not completely exhausted before the plastic melt fronts meet, then a V-notch will form between the plastic and the mold wall. These common defects are often found on the exterior surfaces of welding lines. Not only are they appearance defects, but they also decrease the mechanical strength of the parts. The locations of the welding lines are usually determined by the part shapes and the gate locations. In this paragraph, a heating and cooling system using a vapour chamber was developed. The vapor chamber was installed between the mold cavity and the heating block as shown in Fig. 8. Two electrical heating tubes are provided. A P20 mold steel block and a thermocouple are embedded to measure the temperature of the heat insert device. The mold temperature was raised above the glass transition temperature of the plastic prior to the filling stage. Cooling of the mold was then initiated at the beginning of the packing stage. The entire heating and cooling device was incorporated within the mold. The capacity and size of the heating and cooling system can be changed to accommodate a variety of mold shapes.
According to the experimental results, after the completion of molding, 10% of Type1 samples did not pass torque test, while all Type2 and Type3 samples passed the test. After thermal cycling test, the residual stress of the plastics began to be released due to temperature change, so the strength of product at the position of weld line was reduced substantially. Only 30% of Type1 products passed the 15.82 N-m torque tests after thermal cycling test, followed by 50% of Type2 products and 100% of Type3 products. This study proved that, among existing insert molding process, the temperature of inserts has impact on the final assembly strength of product. In this study, the local heating mechanism of vapor chamber can control the molding temperature of inserts; and the assembly strength can be improved significantly if the temperature of inserts prior to filling can be increased

over the mold temperature, thus allowing the local heating mechanism to improve the weld line in the insert molding process. In this study, a vapour chamber based rapid heating and cooling system for injection molding to reduce the welding lines of the transparent plastic products is proposed. Tensile test parts and multi-holed plates were test-molded with this heating and cooling system. The results indicate that the new heating and cooling system can reduce the depth of the V-notch as much as 24 times.

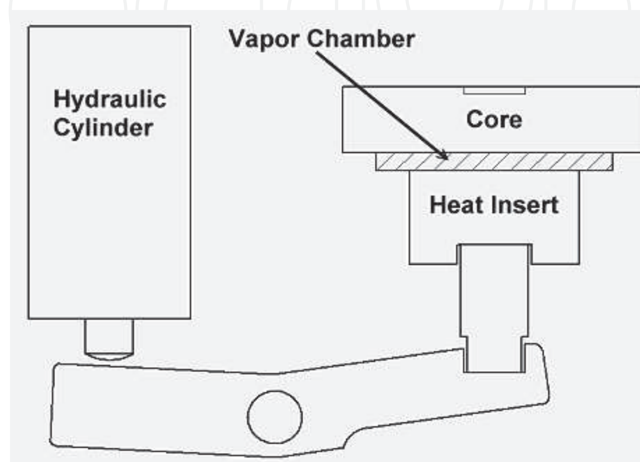

Fig. 8. Mechanics of heating and cooling cycle system with vapor chamber

4.2 Large motor

In this study, the 2350-kW completely enclosed air-to air cooled motor with dimensions 2435mm × 1321mm × 2177mm, as shown in Figure 9, is investigated. The motor includes a centrifugal fan, two axial fans, a shaft, a stator, a rotor, and a heat exchanger with 637 cooling tubes. There are two flow paths in the heat exchanger: the internal and external flows. As shown with the blue arrows, the external flow is driven by the rotation of the centrifugal fan, which is mounted externally to the frame on the motor shaft. The external air flows through the 637 tubes of the staggered heat exchanger mounted on top of the motor. The red arrows in Figure 8 show the internal air circulated by two axial fans on each side of the shaft and cooled by the heat exchanger. This study experimentally and numerically investigates the thermal performance of a 2350-kW enclosed air-to air cooled motor. The fan performances and temperatures of the heat exchanger, rotor, and the stator are numerically determined, which are in good agreement with the experimental data. Due to the non-uniform behaviours of the external air and air leakage of the internal air, the original motor design cannot operate at the best conditions. The designs with modified guide vanes and optimum clearance between the rotor and the axial fan demonstrate that the temperatures of the rotor and stator can decrease 5°C. The new design of the guide vanes makes the flow distributions uniform. Two axial fans with optimal distance operate at the maximum flow rate into the shaft, stator, and rotor, which increases the cooling ability. The present results provide useful information to designers regarding the complex flow and thermal interactions in large-scale motors.

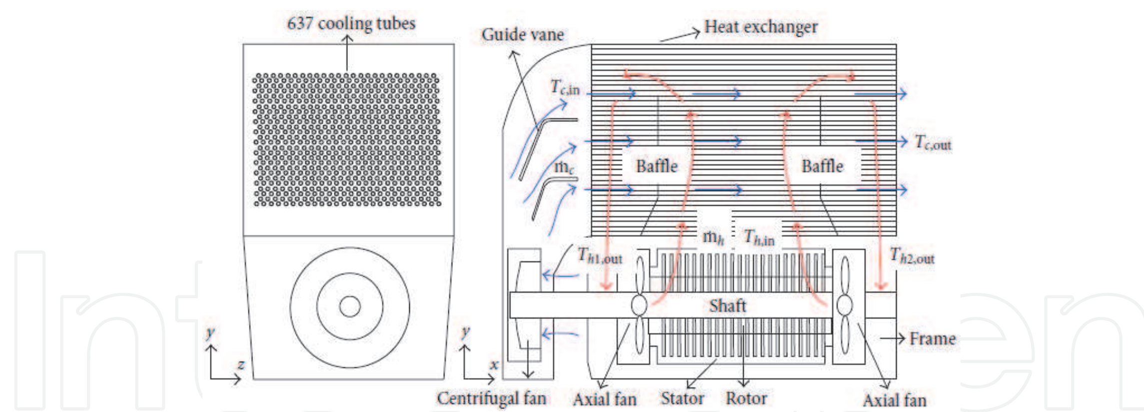

Fig. 9. Schematic view of flow paths and components for the motor.

4.3 LED lighting

The solid-state light emitting diode has attracted attention on outdoor and indoor lighting lamp in recent years. LEDs will be a great benefit to the saving-energy and environmental protection in the lighting lamps region. A few years ago, the marketing packaged products of single die conducts light efficiency of 80 Lm/W and reduces the light cost from 5 NTD/Lm to 0.5 NTD/Lm resulting in the good market competitiveness. These types of LED lamps require combining optical, electronic and mechanical technologies. This article introduces a thermal-performance experiment with the illumination-analysis method to discuss the green illumination techniques requesting on LEDs as solid-state luminescence source application in relative light lamps. The temperatures of LED dies are lower the lifetime of lighting lamps to be longer until many decades. We have successfully applied on LED outdoor lighting lamp as street lamp and tunnel lamp. In the impending future, we do believe that the family will install the LED indoor light lamps and lanterns certainly to be more popular generally.

LED light-emitting principle is put forward by the external bias on the P-Type and N-Type semiconductor, prompting both electron and electricity hole can be located through the depletion region near the P-N junction, and then were into the acceptor P-type and donor N-type semiconductor; and combine with another carrier, resulting in electron jumping and energy level gap in the form of energy to light and heat release, which the carrier concentration and to increase the luminous intensity of one of the factors. Therefore, LED can be a component of converting electrical energy into light energy, including the wavelength of light emitted by the infrared light, visible light and UV. The chemical family group IIIA in the periodic table (B, Al, Ga, IN, Th) and the VA family group (N, P, As, Sb, Bi) or IIA family group (Zn, Cd, Hg) and family group VIA (O, S, Se, Ti, Po) elements composed of compound semiconductor, and connected at the ends to the metal electrode (ohmic contact point), is the basic LED P-N junction structure.

The wavelength of light emitted can be obtained from the formula by Albert Einstein, who used Planck description of photoelectric effect of the quantum theory in 1921. Because the composition of materials for each energy level of semiconductor energy gap is different, its light wavelength generated by them is not the same as shown in Equation (27).

$$\lambda = {(h \times c)}/{E_\lambda} \cong \frac{1.988 \times 10^{-9}}{E'_\lambda}(nm) \cong \frac{1240}{E_\lambda}(nm) \tag{27}$$

Where λ is the light wavelength of LED (nm), h is the Planck constant 6.63 x 10-34 J · s , c is the vacuum velocity of light 2.998 x 10^8 m · s^{-1} and E_λ is the photon energy (eV).
Currently, one of the most serious problems is the thermal management for use of high-power LED lighting lamp, so the overall design and analysis of the thermal performance of LED lighting lamps is important. The following paragraphs will research in the thermal management for some commonly used methods applied to different kinds of LED lighting lamps. The heat-sink numerical analysis is a subject belonging to the computational fluid dynamics (CFD), in which fluid mechanics, discrete mathematics, numerical method and computer technology are integrated. Conventional numerical methods for the flow field are the Finite Element Method (F.E.M.), Finite Volume Method (F.V.M.) and Finite Difference Method (F.D.M.). A vapour chamber has uniquely high thermal performance and an isothermal feature; it has been developed and fabricated at a low-cost due to the mature manufacturing process. Fig. 11 shows a vapor chamber with above 800W/m°C, which is size of 80 x 80 x 3 mm^3 with light weight and antigravity characteristics to substitute for the present fine metal or the embedded heat pipe metal based plate, thus creating a new generation LED based plate. The device reduces the temperature of LEDs and enhances their lifetime. From the Fig.11, the spreading thermal performance of a vapor chamber is obviously better than a Copper plate after 60 seconds at the same operating conditions through thermograph. Its experimental results are shown in Table 1. T_a, T_{vc} and T_{AL} are the temperatures of surroundings, vapour chamber and aluminium based-plate, respectively. R_t is the thermal resistance of vapour chamber-based plate.

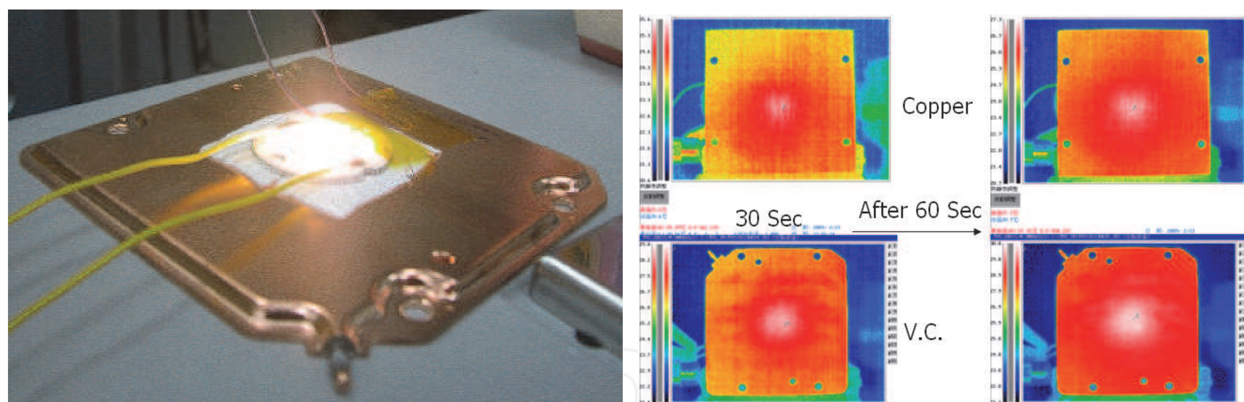

Fig. 10. LED vapour chamber-based plate and temperature distribution

Power (Watt)	Temperature(°C) / Thermal Resistance (°C/W)			
	T_a	T_{vc}	T_{AL}	R_t
5.236	24.5	51	54	5.63
7.100	24.8	68.9	70.9	6.49
8.614	24	75.6	79.2	6.41

Table 1. Experimental result for LED vapour chamber-based plate

Fig. 12 shows the temperature distributions of 12 pieces of LED up to 30Watt AL die-casting heat sink with asymmetry radial fins. A LEDs vapor chamber-based plate is placed on the heat sink and its size is a diameter of 9cm and a thickness of 3mm with thermal conductivity above 1500W/m°C according to the window program VCTM V1.0. To get the numerical results, we supposed that the coefficient of natural convection h is equal to 5W/m²°C and 10W/m²°C and ambient temperature is 25°C. The input power per die is 1.5Watt, 2Watt and 2.5Watt, respectively. Table 2 is the final simulation results.

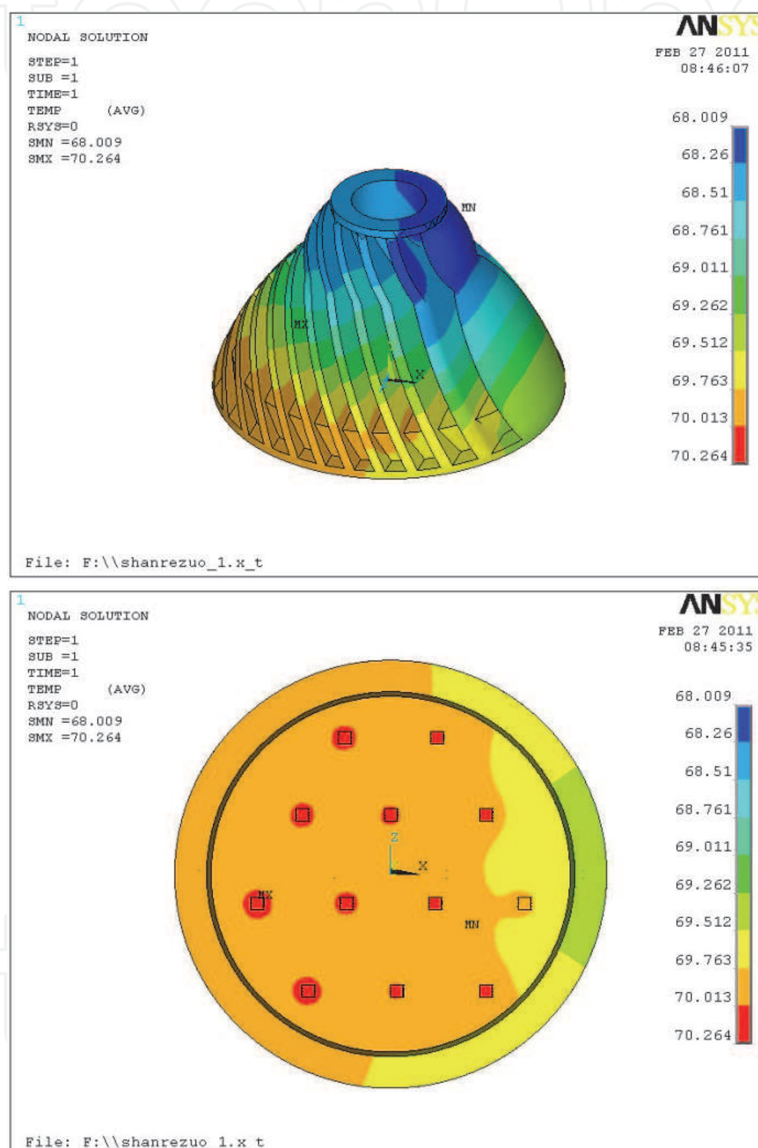

Fig. 11. Temperature distribution of 30 Watt LEDs at h=10

The light bar can be used as indoor living room lighting or outdoor architectural lighting. They are reduced the temperature T_j employed an extruded aluminum strip heat sink. Figure 13 shows a LED table lamp prototype, after a long test, the temperature of internal heat sink at 56°C or less. This table lamp prototype is divided into six parts including lamp body, LEDs, LEDs driver, aluminum based plates, heat sinks and spreading-brightness enhancement film. The illumination of the prototype is 600 lumens (Lm) and the input

power is 12Watt. The luminosity is 1600 Lux measured by a photometer at a distance of 30cm from table lamp. Lastly, according to design and analyze the table lamp prototype, we draw four types of future LED table lamps utilizing above 15Watt or more as shown in Fig. 13. For centuries, all mankind have applied light generated by thermal radiation on many lighting things; now through progress rapidly of semiconductor and solid-state cold light technologies in recent decades, make mankind forward to green environmental protection and energy-saving lighting world in the 21st century. This article describes many indoor and outdoor lighting in features, analysis and design using lot types of heat sinks to address the high-brightness or high-power LEDs combined with optical, mechanical, and electric areas of lighting lamp. The authors are looking for contributing to the LED industry, government and academia for the green energy-saving lamps.

Total Power (Watt)	h=5(W/m²°C)		h=10(W/m²°C)	
	Ave. Temp. (°C)	Max. Temp. (°C)	Ave. Temp. (°C)	Max. Temp. (°C)
18	68.86	69.66	51.48	52.16
24	83.38	84.45	60.25	61.15
30	97.30	98.62	69.14	70.26

Table 2. Simulation situations for AL die-casting heat sink

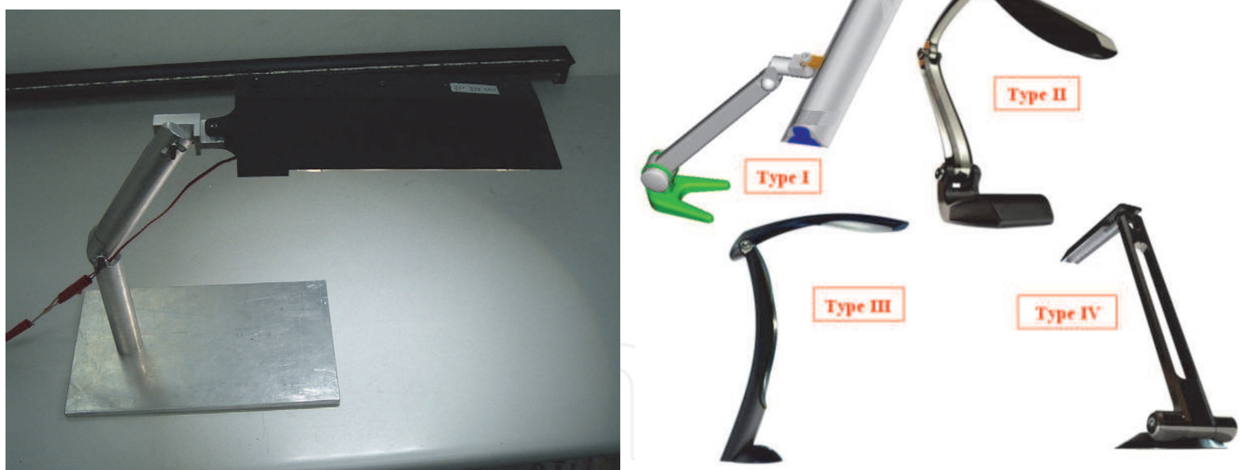

Fig. 12. 3D 12Watt table lamps

5. Conclusion

The air cooling module applies to consumer-electronic products involving automobiles, communication devices, etc. Recently, consumer-electronic products are becoming more complicated and intelligent, and the change occurs faster than ever. To recall the author's early experience in various consumer-electronic products, the heat/thermal problems play an important role in two decades. This chapter investigates all methodologies of Personal Computer (PC), Note Book (NB), Server including central processing unit (CPU) and

graphic processing unit (GPU), and LED lighting lamp of smaller area and higher power in the consumer electronics industry. This approach is expected to help them make decisions related to the lifetime and reliability of their products in a right, reasonable and systematic way. The authors are looking for contributing to the LED industry, government and academia for the green energy-saving lamps. The author's future efforts could be dedicated to developing a LED green energy-saving lamps system. It is also desired that the evaluation method for thermal module be extended to other categories of consumer LED products such as home appliances, office-automation, personal communication devices, automobile interior design, and so on. Finally, the authors would like to mention a few points as the contribution of this study. This can serve as a reference for future researchers.

6. Acknowledgment

This chapter originally appeared in these References and is a major revised version. Some of the materials presented in this chapter were first published in these References. The authors gratefully acknowledge Prof. S.-L. Chen and his Energy Lab., Prof. J.-C. Wang and his Thermo-Illuminanace Lab for guidance their writings to publish and permission to reprint the materials here. The work and finance were supported by National Science Council (NSC), National Taiwan University (NTU) and National Taiwan Ocean University (NTOU). Finally, the authors would like to thank all colleagues and students who contributed to this study in the Chapter.

7. References

Chang, C.-C. ; Kuo, Y.u-F. ; Wang, J.-C. & Chen, S.-L. (2010). Air Cooling for a Large Scale Motor. *Applied Thermal Engineering,* Vol. 30, Issue 11-12, pp.1360-1368.

Chang, Y.-W. ; Cheng, C.-H. ; Wang, J.-C. & Chen, S.-L. (2008). Heat Pipe for Cooling of Electronic Equipment. *Energy Conversion and Management,* Vol. 49, pp.3398-3404.

Chang, Y.-W.; Chang, C.-C.; Ke, M.-T. & Chen, S.-L. (2009). Thermoelectric air-cooling module for electronic devices. *Applied Thermal Engineering,* Vol. 29, No. 13, pp.2731-2737.

Chen, S.-L.; Chang, C.-C.; Cheng, C.-H. & Ke, M.-T. (2009). Experimental and numerical investigations of air cooling for a large-scale motor. *International Journal of Rotating Machinery,* Vol. 2009, Article ID 612723, 7 pages.

Huang, H.-S.; Weng, Y.-C.; Chang, Y.-W.; Chen, S.-L. & Ke, M.-T. (2010). Thermoelectric water-cooling device applied to electronic equipment. *International Communications in Heat and Mass Transfer,* Vol. 37, No. 2, pp.140-146.

Lin, V. & Chen, S.-L. (2003). Performance analysis, optimum and verification for parallel plate heat sink associated with single non-uniform heat source, *ASME 2003 International Electronic Packaging Technical Conference and Exhibition,* InterPACK2003, Vol. 2, pp.229-236.

Tsai, T.-E.; Wu, G.-W.; Chang, C.-C; Shih, W.-P. & Chen, S.-L. (2010a). Dynamic test method for determining the thermal performances of heat pipes. *International Journal of Heat and Mass Transfer,* Vol. 53, No. 21-22, pp.4567-4578.

Tsai, T.-E.; Wu, H.-H.; Chang, C.-C. & Chen, S.-L. (2010b). Two-phase closed thermosyphon vapor-chamber system for electronic cooling. *International Communications in Heat and Mass Transfer,* Vol. 37, No. 5, pp.484-489.

Tsai, Y.-P. ; Wang, J.-C. & Hsu, R.-Q. (2011). The Effect of Vapor Chamber in an Injection Molding Process on Part Tensile Strength. *EXPERIMENTAL TECHNIQUES,* Vol. 35, Issue 1, pp.60-64.

Wang R.-T. & Wang, J.-C. (2011a). Green Illumination Techniques applying LEDs Lighting, *Proceedings of GETM 2011 May 28,* pp.1-7, Changhua, Taiwan.

Wang, J.-C. & Chen, T.-C. (2009). Vapor chamber in high performance server. *Microsystems IEEE 2010 Packaging Assembly and Circuits Technology Conference (IMPACT), 2009 4th International,* pp.364-367.

Wang, J.-C. & Huang, C.-L. (2010). Vapor chamber in high power LEDs. *IEEE 2011 Microsystems Packaging Assembly and Circuits Technology Conference (IMPACT), 2010 5th International,* pp.1-4.

Wang, J.-C. & Tsai,Y.-P. (2011). Analysis for Diving Regulator of Manufacturing Process. *Advanced Materials Research,* Vol. 213, pp.68-72.

Wang, J.-C. & Wang R.-T. (2011b). A Novel Formula for Effective Thermal Conductivity of Vapor Chamber, *EXPERIMENTAL TECHNIQUES,* DOI : 10.1111/j.1747-1567.2010.00652.x, early view.

Wang, J.-C. (2009). Superposition Method to Investigate the Thermal Performance of Heat Sink with Embedded Heat Pipes. *International Communication in Heat and Mass Transfer,* Vol. 36, Issue 7, pp.686-692.

Wang, J.-C. (2008). Novel Thermal Resistance Network Analysis of Heat Sink with Embedded Heat Pipes. *Jordan Journal of Mechanical and Industrial Engineering,* Vol. 2, No. 1, , pp. 23-30.

Wang, J.-C. (2010). Development of Vapour Chamber-based VGA Thermal Module. *International Journal of Numerical Methods for Heat & Fluid Flow,* Vol. 20, Issue 4, pp.416-428.

Wang, J.-C. (2011a). Investigations on Non-Condensation Gas of a Heat Pipe. *Engineering,* Vol. 3, pp.376-383.

Wang, J.-C. (2011b). L-type Heat Pipes Application in Electronic Cooling System. *International Journal of Thermal Sciences,* Vol. 50, Issue 1, pp.97-105.

Wang, J.-C. (2011c). Applied Vapor Chambers on Non-uniform Thermo Physical Conditions. *Applied Physics,* Vol. 1, pp.20-26.

Wang, J.-C. (2011d). Thermal Investigations on LEDs Vapor Chamber-Based Plates. *International Communication in Heat and Mass Transfer,* DOI : 10.1016/j.icheatmasstransfer.2011.07.002, Article in Press, Corrected Proof.

Wang, J.-C. ; Huang, H.-S. & Chen, S.-L. (2007). Experimental Investigations of Thermal Resistance of a Heat Sink with Horizontal Embedded Heat Pipes, *International Communications in Heat and Mass Transfer,* Vol. 34, Issue 8, pp.958-970.

Wang, J.-C. ; Wang, R.-T. ; Chang, C.-C. & Huang, C.-L. (2010a). Program for Rapid Computation of the Thermal Performance of a Heat Sink with Embedded Heat Pipes. *Journal of the Chinese Society of Mechanical Engineers,* Vol. 31, Issue 1, pp.21-28.

Wang, J.-C. ; Wang, R.-T.; Chang, T.-L. & Hwang, D.-S. (2010b). Development of 30 Watt High-Power LEDs Vapor Chamber-Based Plate. *International Journal of Heat and Mass Transfer,* Vol. 53, Issue 19/20, pp.3900-4001.

Wang, J.-C.; Chang T.-L. ; Tsai Y.-P. ; & Hsu R.-Q. (2011a). Experimental Analysis for Thermal Performance of a Vapor Chamber Applied to High-Performance Servers, *Journal of Marine Science and Technology-Taiwan,* Article in Press, Corrected Proof.

Wang, J.-C.; Li, A.-T.; Tsai,Y.-P. & Hsu, R.-Q. (2011b). Analysis for Diving Regulator Applying Local Heating Mechanism of Vapor Chamber in Insert Molding Process. *International Communication in Heat and Mass Transfer,* Vol.38, Issue 2, pp.179-183.

Wu, H.-H.; Hsiao, Y.-Y.; Huang, H.-S.; Tang, P.-H. & Chen, S.-L. (2011). A practical plate-fin heat sink model. *Applied Thermal Engineering,* Vol.31, Issue 5, pp.984-992.

IntechOpen

IntechOpen

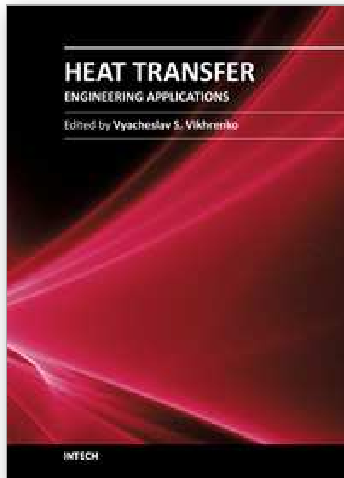

Heat Transfer - Engineering Applications
Edited by Prof. Vyacheslav Vikhrenko

ISBN 978-953-307-361-3
Hard cover, 400 pages
Publisher InTech
Published online 22, December, 2011
Published in print edition December, 2011

Heat transfer is involved in numerous industrial technologies. This interdisciplinary book comprises 16 chapters dealing with combined action of heat transfer and concomitant processes. Five chapters of its first section discuss heat effects due to laser, ion and plasma-solid interaction. In eight chapters of the second section engineering applications of heat conduction equations to the curing reaction kinetics in manufacturing process, their combination with mass transport or ohmic and dielectric losses, heat conduction in metallic porous media and power cables are considered. Analysis of the safety of mine hoist under influence of heat produced by mechanical friction, heat transfer in boilers and internal combustion engine chambers, management for ultrahigh strength steel manufacturing are described in this section as well. Three chapters of the last third section are devoted to air cooling of electronic devices.

How to reference
In order to correctly reference this scholarly work, feel free to copy and paste the following:

Jung-Chang Wang and Sih-Li Chen (2011). Air Cooling Module Applications to Consumer-Electronic Products, Heat Transfer - Engineering Applications, Prof. Vyacheslav Vikhrenko (Ed.), ISBN: 978-953-307-361-3, InTech, Available from: http://www.intechopen.com/books/heat-transfer-engineering-applications/air-cooling-module-applications-to-consumer-electronic-products

INTECH
open science | open minds

InTech Europe
University Campus STeP Ri
Slavka Krautzeka 83/A
51000 Rijeka, Croatia
Phone: +385 (51) 770 447
Fax: +385 (51) 686 166
www.intechopen.com

InTech China
Unit 405, Office Block, Hotel Equatorial Shanghai
No.65, Yan An Road (West), Shanghai, 200040, China
中国上海市延安西路65号上海国际贵都大饭店办公楼405单元
Phone: +86-21-62489820
Fax: +86-21-62489821

© 2011 The Author(s). Licensee IntechOpen. This is an open access article distributed under the terms of the Creative Commons Attribution 3.0 License, which permits unrestricted use, distribution, and reproduction in any medium, provided the original work is properly cited.

IntechOpen

IntechOpen